View metadata, citation and similar papers at core.ac.uk

brought to you by CORE

provided by UT Digital Repository

Copyright

by

Eunsoo Yoon

2017

The Thesis Committee for Eunsoo Yoon
Certifies that this is the approved version of the following thesis:

Photoelectrochemical Ion Concentration Polarization: a microfluidic ion filtration system using light-driven electrochemical reactions.

APPROVED BY
SUPERVISING COMMITTEE:

Supervisor:

Richard M. Crooks

Charles B. Mullins

Photoelectrochemical Ion Concentration Polarization: a microfluidic ion filtration system using light-driven electrochemical reactions.

by

Eunsoo Yoon, B.S.

Thesis

Presented to the Faculty of the Graduate School of

The University of Texas at Austin

in Partial Fulfillment

of the Requirements

for the Degree of

Master of Arts

The University of Texas at Austin

May 2017

Dedication

To my family, Jeongbong Yoon, Junghee Jung, and Changhoon Yoon.

Acknowledgements

I gratefully acknowledge my supervisor, Richard M. Crooks, for allowing me to work in his lab for three years and giving me advice for the works; Tim Hooper for setting up instruments for experiments; and our funding agent.

Abstract

Photoelectrochemical Ion Concentration Polarization: a microfluidic ion filtration system using light-driven electrochemical reactions.

Eunsoo Yoon, M.A.

The University of Texas at Austin, 2017

Supervisor: Richard M. Crooks

We report an ion separation or filtration method used in microchannel called photoelectrochemical ion concentration polarization (pICP). As a variant of faradaic ion concentration polarization (fICP), pICP utilizes TiO_2 photoelectrochemistry to form an ion depletion zone (IDZ) with light. A microfluidic device with TiO_2 photoanode and Pt cathode generated IDZ near the cathode by generating a corresponding electrochemical reaction. Local electric field near the cathode was amplified with TiO_2 irradiation. Furthermore, on-chip solution conductivity measurement confirmed decrease in ion concentration as a consequence of pICP ion filtration.

Table of Contents

List of Figures

List of Illustrations

Chapter 1. Introduction

1.1 Ion Concentration Polarization (ICP)

Ion concentration polarization (ICP) is a general method for manipulating ions in solution,[1–3] especially in the microchannel systems for preconcentrating charged molecules. The main principle for ICP implementation is shown as Illustration 1.1 a.[4–8] Here, two fluidic channels are separated by a negatively charged nanochannel or permselective membrane. When a driving voltage (V_D) is applied with the indicated polarity, cations are driven from the top channel, through the ion-selective channel or membrane, and into the bottom channel. Anions in the top channel then migrate toward the positive driving electrodes. This action results in formation of an ion depletion zone (IDZ) near the intersection of the top and ion-selective channels, and an ion enrichment zone (IEZ) near the intersection of the bottom and ion-selective channels. Increased solution resistivity in the IDZ results in elevated local electric field at the region. The high local electric field has been utilized for electrokinetically manipulating charged molecules.

Analyte preconcentration[9–13] is one of the most representative applications of ICP. For example, we previously observed DNA preconcentrated near the IDZ which was formed by a nanoporous polyester membrane.[4] Other important uses of ICP probably includes partial desalination of water.[14,15] For example, Han and coworkers reported ICP-based partial desalination of salt water in a microfluidic device featuring a Nafion permselective membrane as the active component.[14] Sinton and coworkers reported a similar approach, but they used a three-dimensional fluidic system to improve efficiency.[15] Recently, ICP applications have even been adapted to paper fluidic devices[16,17] for enrichment and detection of biomolecules.[10,11,13]

Besides its applicability for the electrokinetic ion manipulations, unique vortical flow formed in ICP system was extensively studied.[18–22] It was revealed due to a secondary electroosmotic flow generated near the IDZ.[22] Also the ICP was reported to have three different unique stages of current-voltage (I-V) regime, which are ohmic, limiting and over-limiting. The vortical flow is known to result in the over-limiting I-V regime by generating the non-linear convection near the IDZ.[19,21] The unique properties of ICP have also been used to construct micromixers[23,24] and ionic diodes and transistors.[25]

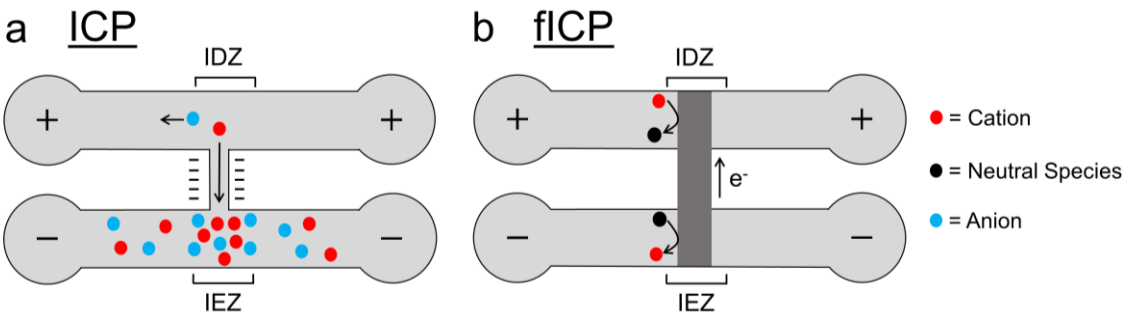

Illustration 1.1: Schemes for ICP and fICP.

1.2 Faradaic Ion Concentration Polarization (fICP)

Several years ago we introduced an electrochemical version of ICP that we call faradaic ICP (fICP). Instead of using ion selective membrane, electrochemical reactions enabled selective ion transport between two channels to form IDZ and IEZ. As shown in Illustration 1.1 b, the experimental configuration for fICP is similar to that used for normal ICP with the exception that the permselective nanochannel or membrane is replaced by a bipolar electrode (BPE).[26–29] In this case, an electroactive cation in the top channel is electrochemically reduced to a neutral species, and in the bottom channel a neutral species is oxidized to form a cation. The net effect is that an IDZ forms near the cathode of the BPE in the top channel, and an IEZ forms near the BPE anode in the bottom channel.

Briefly explaining about the BPE, it works slightly different from the conventional electrochemical cell which generates faradaic reaction when potential is directly applied between the anode and the cathode. In the BPE system (Illustration 1.2), however, the potential is applied to the electrolyte through the driving electrodes and the potential difference between the ends of the BPE drives the faradaic reactions. Note that the BPE is a conductive material sitting in the electrolyte without direct connection to the power source. There are several benefits of using the fICP instead of the ICP. First, fabrication of microfluidic device becomes much facile without using membrane. Second, it prevents problems involved in using membrane, such as a membrane fouling. Third, it requires lower energy to generate the IDZ. This is because the ion transport is limited by the electron-transport rather than the mass-transport.

Ever since we first observed the fICP,[30] its fundamental principles have been extensively studied.[31–34] We have demonstrated that ion enrichments,[30,33–35] separation,[36,37] depletion[38], and gating[39] can be operated in the buffer electrolytes using

the fICP. Later, the sea water desalination was demonstrated by electrochemically depleting chloride ions in the sea water electrolyte.[40] Most recently, it was confirmed that the fICP can be applicable as a preconcentration method in a paper fluidic device by enriching biomolecules and nanoparticles.[41]

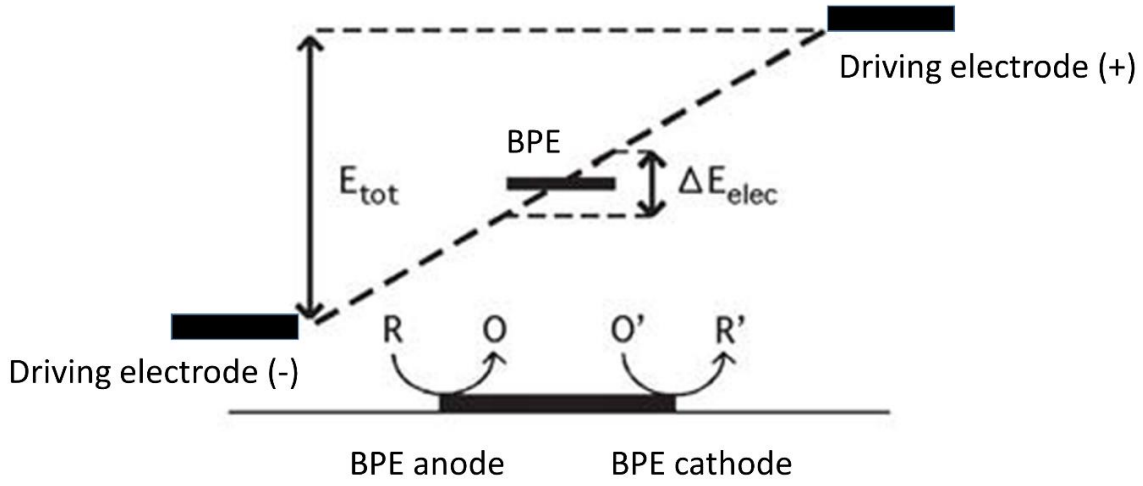

Illustration 1.2: Principle of generating faradaic reactions on the bipolar electrode (BPE).

1.3. ACHIEVEMENT AND SUMMARY

In the present thesis we introduce a new version of ICP called photoelectrochemical ICP, or pICP. This method is similar to fICP, but in this case the IDZ is generated primarily by light energy rather than by a power supply. The experimental arrangement for pICP is shown in Illustration 1.3 a and b. This is a typical two-electrode microelectrochemical cell configuration with a TiO_2 photoanode photolithographically defined at the bottom of the inlet reservoir of the device and a Pt microband cathode situated within the channel. The key point is that when the photoanode is illuminated, a corresponding faradaic electrochemical reaction is driven at the Pt cathode that results in formation of a local IDZ.

Regardless of whether the IDZ forms by ICP, fICP, or pICP, it has some characteristics in common. The most important of these is illustrated in Illustration 1.3 c specifically for pICP, but it applies to the other methods as well. Here, the local IDZ results in a region of high electric field near the Pt cathode. When anions enter the IDZ they are accelerated by this higher field toward the photoanode by electromigration. If there is an opposing convective force, which in this case is pressure-driven flow (PDF) enabled by a difference in the height between the solutions in the two reservoirs (Illustration 1.3 a), then anions feel the difference between the two forces. For example, anions in the weakest part of the local electric field gradient experience a net velocity from left to right, and those in the strongest part of the field move from right to left. The net effect is that anions are swept into a single location where their velocity sums to zero. In other words, anions are focused and concentrated at this single position within the microchannel. Techniques in which two forces oppose each other to drive ions to a single location are generally known as electric field gradient focusing (EFGF) methods.[42,43]

Herein, we describe the experimental approach for implementing pICP, and use in-situ electric field measurements to confirm the presence of a light-generated IDZ. We show that this approach can be used to partially desalinate water and measure solution conductivity to confirm it. Finally, the ion filtration is visualized using the fluorescent ion tracers.

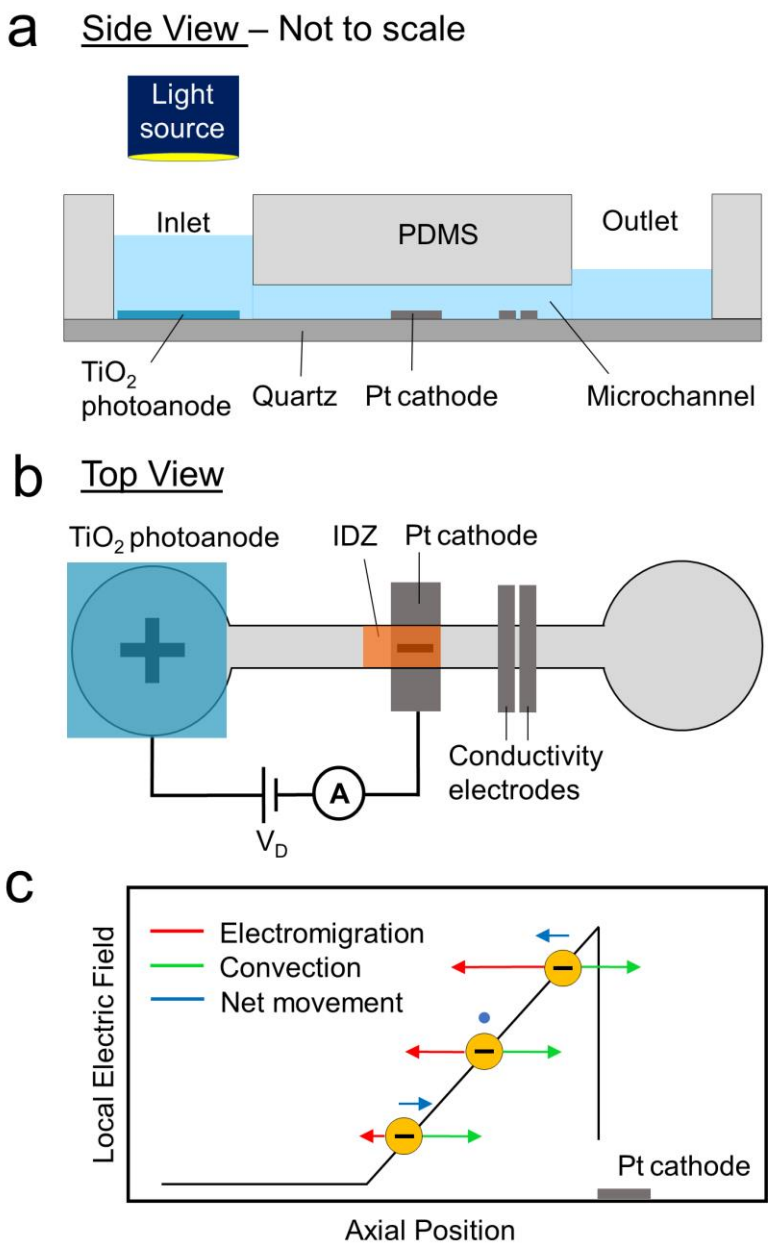

Illustration 1.3: Schemes of a pICP device and its basic principle. (a) Side view of the pICP device. (b) Top view of the pICP. (c) Local electric field profile near the Pt cathode and resulting anion enrichment.

Chapter 2. Experimental Section

2.1 CHEMICALS AND MATERIALS

The acidic and basic forms of Tris were obtained from Sigma-Aldrich (St. Louis, MO). A 100 mM Tris buffer solution was prepared by mixing approximately equal amounts of the two forms of Tris in deionized water (DI water, 18.0 MΩ·cm, Milli-Q Gradient System, Millipore), and then titrating to pH 8.0. Different concentrations of these Tris-HCl solutions (50.0 mM, 20.0 mM, 10.0 mM, and 1.0 mM) were prepared by diluting the 100 mM stock solution with DI water.

Quartz microscope slides were purchased from Technical Glass Products, Inc. (Painesville Twp., Ohio). H_2O_2 (30%), H_2SO_4 (98%), Cu wire, and acetone (HPLC grade) were obtained from Fisher Chemical. Adhesion promoter (Micro Prime HP Primer, Shin-Etsu MicroSi, Phoenix, AZ), positive tone photoresist (AZ 1518, AZ Electronic Materials, Somerville, NJ), and developer (AZ 400K, AZ Electronic Materials) were used for photolithography. Ethanol was from PHARMCO-AAPER (Brookfield, CT) and Ag paste was from Electron Microscopy Sciences (Hatfield, PA). Carboxyl-functionalized polystyrene microspheres having a diameter of 0.99 μm (PC04N, Bangs Laboratories, Inc., Fishers, IN) were used as tracers.

2.2 DEVICE FABRICATION

The hybrid PDMS/quartz microfluidic device (hereafter, the 'microelectrochemical cell') was fabricated following a previously reported method.[44] Briefly, TiO_2 and Pt microband electrodes were patterned in separate steps on quartz slides using standard photolithographic techniques. Specifically, the slides were immersed in piranha solution (1:3 H_2O_2/H_2SO_4; *caution: piranha reacts violently with*

organic chemicals and it should be handled in a ventilated hood with extreme care) for 15 min, followed by rinsing with DI water. Next, an adhesion promoter and photoresist were spin-coated onto the slides. The photoresist was then exposed to UV light through a mask. Finally, the pattern was developed in the resist.

Next, 210 nm of Ti (Kurt J. Lesker Company, Jefferson Hills, PA) was deposited by electron-beam physical vapor deposition. Photoresist lift-off was performed by sonicating the substrate in acetone, leaving behind the desired electrode pattern on the quartz slides. The patterned Ti electrode was converted to TiO_2 by thermal oxidation under flowing air in a tube furnace (Model 55035, Lindberg, Riverside, MI).[45] The temperature was ramped from 25 °C to 450 °C at a rate of 30 °C/min and then held at 450 °C for 1.0 h. After oxidation, the substrates were cooled to 25 °C at a rate of 5.0 °C/min. The Pt (Kurt J. Lesker Company, Jefferson Hills, PA) electrodes (100 nm Pt plus 15 nm Ti adhesion layer) were patterned using the same procedure, but without thermal oxidation.

The PDMS microchannel (6.0 mm long, 100 μm wide, and 20 μm high) was fabricated by soft lithography using a Sylgard 184 silicone elastomer kit (Dow Corning Corporation, Midland, MI) and a SU-8 (MicroChem, Westborough, MA) mold patterned on a Si wafer. Inlet and outlet reservoirs (4.0 mm diameter) were punched into the PDMS, and then it was rinsed with ethanol and dried with flowing N_2. The quartz slide and the PDMS channel were exposed to an O_2 plasma (Model PDC-32G, Harrick Scientific, Ossining, NY, 45 s, medium power setting), and then brought into contact. The assembled microelectrochemical cell was immediately placed in 65 °C oven for 5.0 min to promote irreversible bonding between the PDMS and quartz.

2.3 CHARACTERIZATION OF THE TiO_2 ELECTRODE

To fully characterize the TiO_2 microband electrodes, it was necessary to prepare analogs having macroscopic lateral dimensions. Accordingly, 210 nm- and 50 nm-thick TiO_2 thin films were deposited and thermally processed identically to the electrode used for pICP in the microelectrochemical device. These films were then characterized by X-ray diffraction (XRD, Rigaku Ultima IV, Rigaku Americas Corp., The Woodlands, TX) and UV-vis spectroscopy (Cary 5000 UV-vis-NIR spectrometer, Agilent, Santa Clara, CA) as shown in Figures 2.1 and 2.2, respectively.

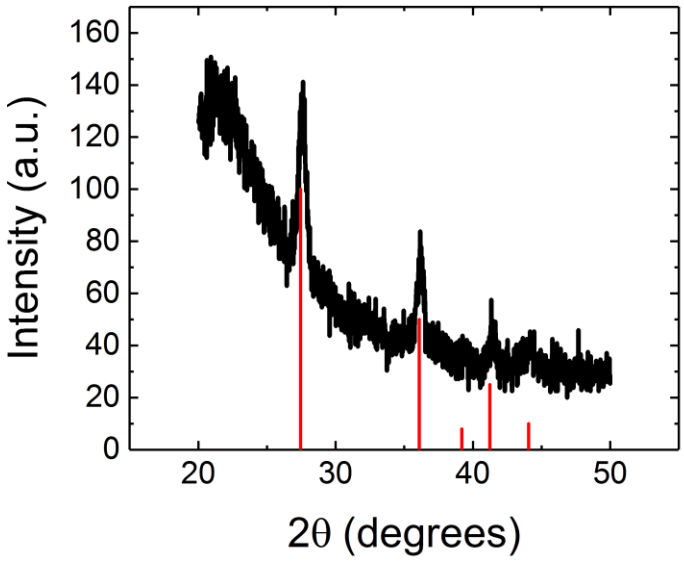

Figure 2.1: XRD spectrum of a TiO_2 thin film on a quartz substrate. A 210 nm-thick TiO_2 thin film having macroscopic lateral dimensions was prepared identically to the electrodes used for pICP in the microelectrochemical device and analyzed using a Rigaku Ultima IV diffractometer (Rigaku Americas Corp., The Woodlands, TX). The spectrum matches the characteristic diffraction peaks of rutile TiO2 (JCPDS: 00-021-1276), which are shown in red. The sloping background continuum arises from the fused quartz substrate.

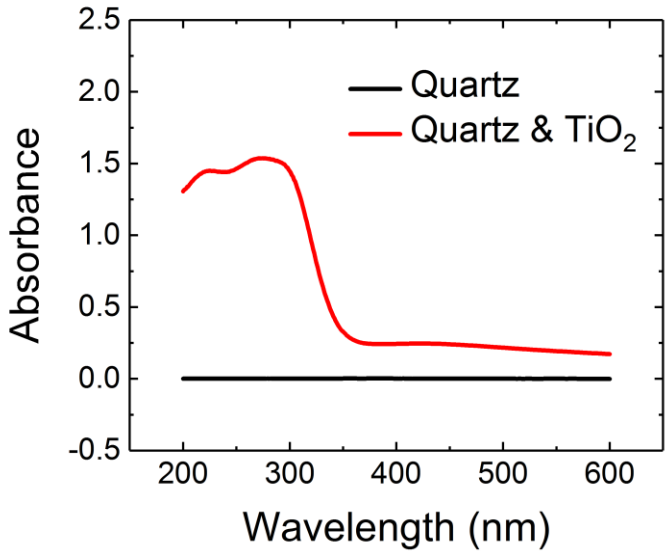

Figure 2.2: UV-vis spectra of a TiO_2 thin film on a quartz substrate and a quartz-only substrate. A 50 nm-thick TiO2 thin film having macroscopic lateral dimensions was prepared identically to the electrode used for pICP in the microelectrochemical device. The spectra were obtained using a Cary 5000 UV-vis-NIR spectrometer (Agilent, Santa Clara, CA).

The photoelectrochemical properties of macroscopic TiO_2 thin films were examined using a macroscopic Teflon cell configured with the TiO_2 working electrode defined by a 4.0 mm-diameter O-ring at the bottom of the cell. The counter electrode was a Pt wire and the electrolyte solution was 100 mM Tris buffer (pH 8.0). A power supply (Model LLS9120, TDK-Lamda Americas, Inc., San Diego, CA) and ammeter (Model 6517B electrometer, Keithley Instruments, Inc., Cleveland, OH) were connected in series between the TiO_2 and counter electrodes. The photocurrent was measured as a function of the applied bias and light intensity. The photocurrent arising from a Pt thin film working electrode was also measured as a control. A 100 watt Hg arc lamp (Model OmniCure s1000, Lumen Dynamics, Ontario, Canada) configured with a 320 – 500 nm filter and a fiber optic were used to irradiate the electrodes. For photoelectrochemical

measurements, the tip of fiber was placed 2.5 cm away from the thin film electrodes. The intensity of the light at this distance was calculated to be ~65 W/cm^2. Details of the measurement and a spectrum of the lamp emission are provided in Figure 2.3.

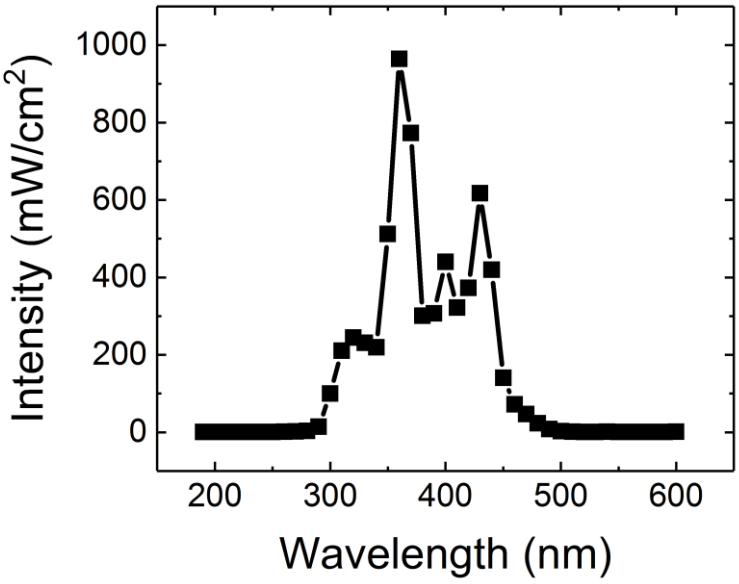

Figure 2.3: Plot of the incident light intensity from the Hg arc lamp vs wavelength. The total irradiance was measured at a distance of 2.5 cm from the lamp (the same distance used for pICP experiments). The measurements were made using a photodetector (Model 818-UV, Newport, Irvine, CA), a monochromator (Newport), and power meters (Models 1830-C and 843-R). The spectral irradiance was measured between 190 nm and 600 nm at 10 nm intervals. By integrating the area under the curve, the total irradiance was found to be ~65 W/cm^2.

2.4. ELECTRIC FIELD MEASUREMENTS

As previously described,[31,32] the longitudinal electric field profile within the channel was monitored using a scanning digital multimeter (SDMM, Model 2700, Keithley Instrument Inc., Cleveland, OH) equipped with a multiplexer module (Model 7701, Keithley). The multiplexer was connected to Pt microbands present near the Pt cathode in the microchannel. The SDMM was used to sequentially read the voltage difference between pairs of neighboring microbands. The acquisition time for each voltage measurement was ~0.10 s, and the voltage at each position within the microchannel was measured every 2.0 s.

2.5 ON-CHIP CONDUCTIVITY MEASUREMENT

The apparatus used for in-situ conductivity measurements is based on a previously reported design.[40,46] Briefly, a pair of 20 μm-wide Pt microband electrodes separated by a 20 μm gap was patterned on the quartz base of the microelectrochemical device concurrent with photolithographic fabrication of the Pt cathode. A function generator (Model 182A, Wavetek, San Diego, CA) applying a sinusoidal ac voltage (~100 kHz frequency, ± 0.30 V amplitude) across the two microbands. Thus, the function generator was connected to one of the microbands labeled as *A* in Illustration 2.1. The resulting ac current signal is determined primarily by the solution conductance, which in turn is proportional to the concentration of charge carrier (eq 1).

$$L = \frac{A}{l}\sum \lambda_i c_i \qquad (1)$$

Here, L is the solution conductance, A is the electrode area, l is the distance between electrodes, λ_i is the molar conductivity of ion i, and c_i is its concentration.[47] The other microband electrode (microband *B* in the Illustration 2.1) was connected to a home-built circuit board with on-board transimpedance amplifiers. This circuit received and

amplified the current resulting from the input voltage and converted it into a voltage signal. The output from the circuit board was connected to a multifunctional PC data acquisition board (Model NI PCI-6229, National Instruments, Austin, TX) through a connector block (Model SCB-68A, National Instruments). The input signal was digitally processed by the data acquisition board and provided the average peak-to-peak amplitude of the ac signal in LabVIEW software.

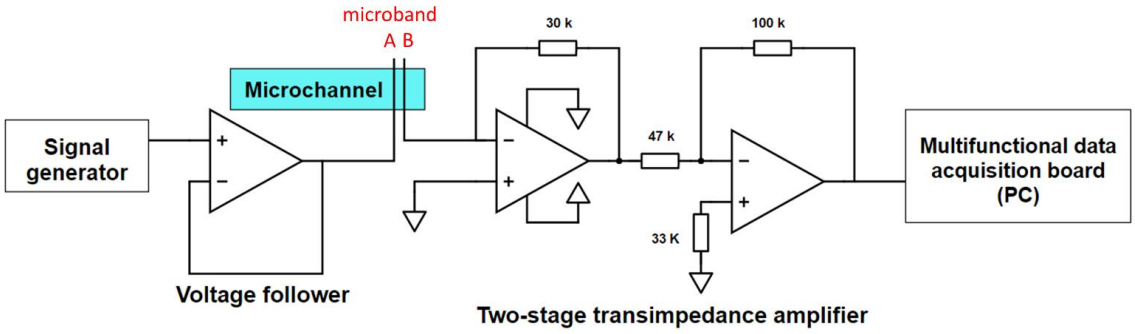

Illustration 2.1: Schematic diagram of the conductivity measurement electronics.

Chapter 3. Results and Discussion

3.1 pICP OPERATION

As discussed in detail in the Experimental Section, pICP was performed using the hybrid PDMS/quartz microelectrochemical device shown in Illustration 1.3a and b. To set up the experiment, the tip of a fiber optic connected to a Hg arc lamp was positioned 2.5 cm away from the TiO_2 electrode configured on the floor of the inlet reservoir. PDF was generated by introducing 40 μL and 34 μL of 100 mM Tris buffer into the inlet and outlet reservoirs, respectively, as shown in Illustration 1.3a. A power supply and ammeter were placed in series with the electrodes as shown in Illustration 1.3b.

When the power supply and light are activated, water is oxidized at the TiO_2 anode (eq 1) and reduced at the Pt cathode (eq 2). In a following reaction, electrogenerated OH^- neutralizes $TrisH^+$ present near the Pt cathode (eq 3).[33] The net result of these processes is that an IDZ forms near the Pt cathode (Illustration 1.3b, burnt orange rectangle). As discussed earlier, this results in a region of high solution resistance and a co-located local electric field gradient (Illustration 1.2 c).

Anode: $$2H_2O \rightarrow 4H^+ + O_2 + 4e^- \quad (1)$$

Cathode: $$2H_2O + 2e^- \rightarrow 2OH^- + H_2 \quad (2)$$

$$OH^- + TrisH^+ \rightarrow Tris + H_2O \quad (3)$$

3.2 CURRENT RESPONSE OF THE TiO_2 PHOTOANODE

On the basis of our previous results relating to fICP,[32,33] we know that the magnitude of the current has a dominant effect on the properties of the IDZ and hence the transport of ions. Accordingly, we characterized the photoelectrochemical properties of

TiO_2 electrodes as a function of V_D and the light intensity at the photoanode. As a control, the same measurements were made for a photo-insensitive Pt electrode. As discussed in detail in the Experimental Section (Chapter 2), these preliminary electrochemical measurements were carried out using macroscopic electrodes, a macroscopic, two-electrode cell, and a solution containing 100 mM Tris buffer (pH 8), which is the same buffer used previously for fICP.[30–32,39]

Figure 3.1a is a plot of current density vs time for a TiO_2 macroscopic electrode in the absence and presence of light. In this case, no V_D was applied, and the photocurrent density was ~0.20 mA/cm^2. On rutile TiO_2, this current results from water oxidation (eq 1) at the TiO_2 electrode and water reduction (eq 2) at the Pt wire counter electrode.[48,49]

We next carried out measurements like those in Figure 3.1a, but as a function of V_D (Figure 3.1b). There are two key results that will become important when the microelectrochemical data are discussed. First, the current density increases monotonically in the presence of light, and, second, it is close to zero when the light is off over the range of V_D values examined.[50,51] The data in Figure 3.1c were obtained by carrying out an experiment identical to that just described for Figure 3.1b, except that the illuminated anode was Pt rather than TiO_2. In this case the current densities track each other regardless of illumination, but the magnitude for the light-on case is more than 10-fold lower than in Figure 3.1b. Note that the current density is slightly higher on Pt than for TiO_2 when the light is off, but this is simply a consequence of the Pt anode being a good electrocatalyst for water oxidation.[52] The important conclusion from Figure 3.1 is that the TiO_2 photoanode yields a substantial current under illumination at low values of V_D. This lowers the overall electrical energy required to drive a process like ICP-induced desalination.[40,14,15]

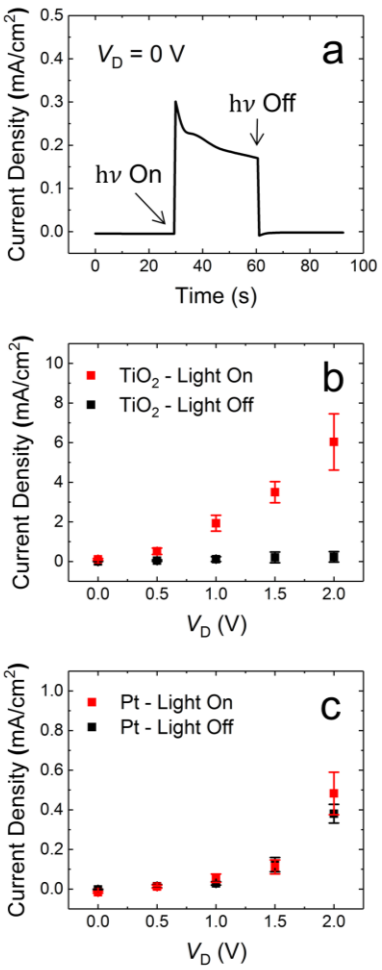

Figure 3.1: Plots of photocurrent density as a function of time and driving voltage (V_D). All data were obtained using a macroscale, two-electrode Teflon cell containing 100 mM Tris buffer (pH 8.0). The counter electrode was a Pt wire. (a) Plot of photocurrent density vs time obtained using a TiO_2 photoanode illuminated with a Hg arc lamp. V_D = 0 V. (b) Plot of photocurrent density vs V_D in the presence and absence of light. The photoanode was a TiO_2 thin film. (c) Plot of current density vs V_D in the presence and absence of light. For this control experiment, the working electrode was a Pt thin film. The current density has been normalized to the area of each thin film. For (b) and (c) the steady-state current density was measured 30 s after applying V_D and, where relevant, light. The error bars represent the standard deviation from the mean for three measurements using independently fabricated Pt or TiO_2 thin films.

3.3 MEASUREMENT OF THE LOCAL ELECTRIC FIELD

As discussed in the Introduction, fICP requires formation of a local electric field. Accordingly, we confirmed the presence of this field in the microelectrochemical cell and measured its dependence on both illumination and V_D using an approach we have previously reported.[31,32,35,36,38] Specifically, Pt microbands 1 – 6 (Figure 3.2a) were configured in the vicinity of the Pt cathode (microband *P*), and a scanning digital multimeter (SDMM) was used to measure the voltage difference between pairs of neighboring microbands. The experiment was carried out as follows. First, the microfluidic device was filled with 100 mM Tris buffer (pH 8.0) and set up for pICP operation as discussed earlier. Second, the SDMM was attached to the numbered microbands to measure the local electric field. Third, V_D was applied to the microelectrochemical device, and in some cases the TiO_2 electrode was illuminated.

Figure 3.2b is a plot of the local electric field profile along the long axis of the microchannel and in the vicinity of the Pt cathode in the absence of light. Position 0 on the horizontal axis is the location of the Pt cathode, and the indicated distances are measured toward the photoanode. These distances represent the midpoint between pairs of adjacent microband electrodes. The important point is that in the absence of light, even at V_D = 2.0 V, a negligible local electric field gradient is observed. This result is consistent with the data in Figure 3.1b, which shows that only a very small current passes between the photoanode and cathode in the absence of light.

Figure 3.2c is analogous to Figure 3.2b, but in this case the TiO_2 photoanode is illuminated. When V_D = 0 V, there is still no appreciable local electric field, because V_D alone is insufficient to create an IDZ. However, when V_D = 0.50 V, a slight increase in the local field is observed near the Pt cathode. At higher values of V_D, a more significant local electric field emerges. For example, when V_D = 2.0 V, the maximum field is ~9

kV/m. These findings are consistent with the results in Figure 3.1b, which shows a steady increase in current (and hence neutralization of buffer by OH^-) as V_D increases. Importantly, we have previously shown that a local electric field ~5.0 kV/m is sufficient to deplete fluorescent ion tracers,[38] although the specific value for a particular experiment depends on the rate of convection.

Figure 3.2d is a plot of the photocurrent density measured concurrently with the data shown in Figure 3.2c. The values of V_D used for each measurement are provided in the figure. Each V_D was applied for 1.0 min with a 1.0 min time interval between measurements. The general trends of these photocurrents are similar to those found for macroelectrodes (Figure 3.1b), but there is a decrease in current toward the end of the current transients for V_D = 1.5 V and 2.0 V. There are two possible explanations for the latter observation. First, an increase in solution resistance (R) in the IDZ increases the voltage drop in the solution between the photoanode and the cathode. This voltage drop is proportional to iR, where i is the current. The increase in the voltage dropped in the solution reduces the interfacial potential difference for each electrode and hence the current. A similar observation has been reported during fICP.[32] Second, the rate of water reduction (eq 2) at the cathode could decrease due to electrogeneration of OH^- and the corresponding local pH change. This scenario is less likely, however, because the solution is buffered.

One final point should be mentioned. Although all the microelectrochemical devices exhibited electric field gradients for V_D > 0.50 V, there were substantial device-to-device variations in their size and shape. For example, at V_D = 0.50 V, the magnitude of the gradient near the cathode varied by as much as ±50% (standard deviation based on measurements from four independent devices). At present, the two most difficult variables to control reproducibly are the TiO_2 photocurrent response and the PDF rate.

With regard to the latter, recall that PDF is generated by controlling the volume of solution in the two reservoirs. However, slight device-to-device variations in the dimensions of these reservoirs result in different solution heights and hence different flow rates. These variations between experiments do not detract from the main finding, which is that light can be used to electrogenerate the IDZ.

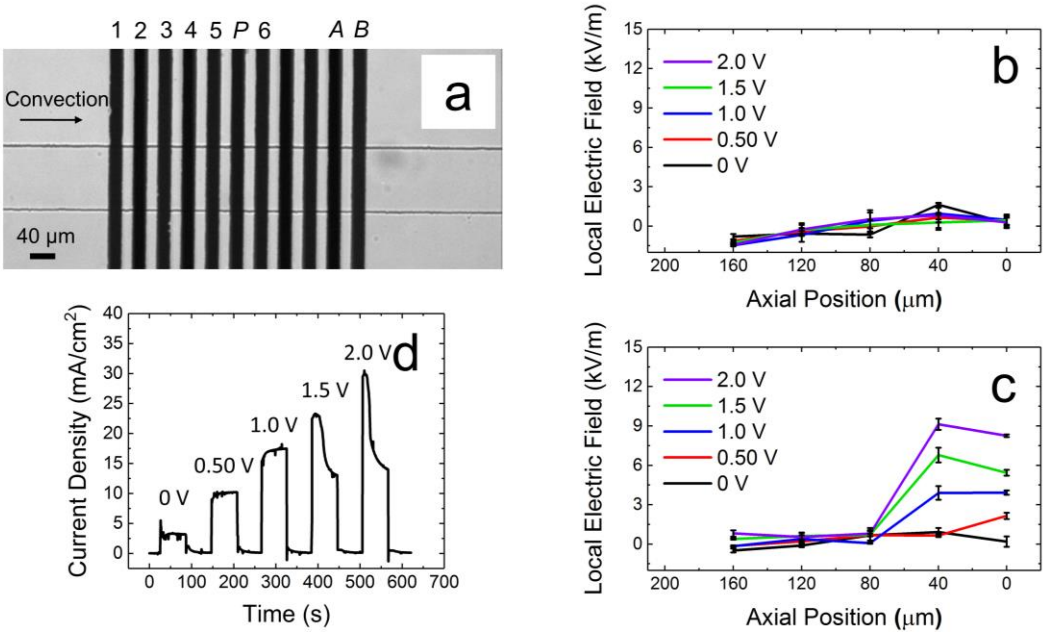

Figure 3.2: (a) Optical micrograph of a microchannel in the vicinity of the Pt cathode. The numbered Pt microbands were used for electric field measurements. The Pt cathode is labeled *P*, and microbands *A* and *B* were used for conductivity measurements. All data were obtained using a pICP device containing 40 µL and 34 µL of 100 mM Tris buffer (pH 8.0) in the inlet and outlet reservoirs, respectively. The TiO_2 photoanode (not shown) was positioned at the bottom of inlet reservoir and was illuminated with an Hg arc lamp. V_D was applied between the Pt cathode and the TiO_2 photoanode. Each value of V_D was applied for 1.0 min with a 1.0 min interval (at open circuit) between measurements in the sequence: 0 V, 0.50 V, 1.0 V, 1.5 V, and 2.0 V. (b) Plot of average local electric field strength vs position in the absence of light and as a function of V_D. (c) Plot of average local electric field strength vs position in the presence of light and as a function of V_D. For (b) and (c), position 0 denotes the location of the Pt cathode, and the indicated distance are increasing in the direction of the photoanode. The values of the electric field strength were averaged for the last 10 s of the 1 min application of V_D (and where relevant, light). The error bars represent the standard deviation from the mean for 5 measurements made over the 10 s period in a single device. (d) Plot of photocurrent density measured concurrently with the data shown in (c). The total current has been normalized to the area of the Pt cathode.

3.4 ON-CHIP CONDUCTIVITY MEASUREMENT

Consider the microelectrochemical device shown in Illustration 1.2b, and particularly the relationship between the IDZ and the conductivity measurement electrodes. In the previous section we confirmed the presence of the IDZ, and therefore we expect the associated electric field gradient will resist the passage of ions as shown in Illustration 1.3c. This means that ions will concentrate to the left of the IDZ, and consequently the conductivity of the solution downstream of the Pt cathode should be lower than that of the feed stream. We tested this hypothesis by measuring the downstream conductivity.

Microbands *A* and *B* (Figure 3.2a) positioned ~180 μm downstream of the Pt cathode (microband *P*) and the measurement circuit shown in Illustration 2.1 were used to determine the local solution conductivity in the microelectrochemical cell. Figure 3.3a is a calibration curve constructed using the following concentrations of Tris buffer (1.0 mM, 10.0 mM, 20.0 mM, 50.0 mM, and 100 mM, pH 8.0) in the microelectrochemical device in the absence of light and with V_D = 0 V. Because the conductivity signal only depends on the concentration of charged species, the calibration curve is presented in terms of $TrisH^+$ concentration. The measured conductivity signals are linearly proportional to the $TrisH^+$ concentration.

Figure 3.3b is a plot of the concentration of $TrisH^+$ as a function of time during pICP with V_D = 0 V. This plot was constructed by measuring the solution conductivity using the conductivity electrodes, and then converting conductivity to $TrisH^+$ concentration using the calibration curve in Figure 3.3a. For this experiment, the initial $TrisH^+$ concentration determined by in-situ solution conductivity was 51.3 mM. This can be compared to the nominal $TrisH^+$ concentration of 54.0 mM. The difference in

magnitude between these two values is typical of the intrinsic error associated with the conductivity measurement.

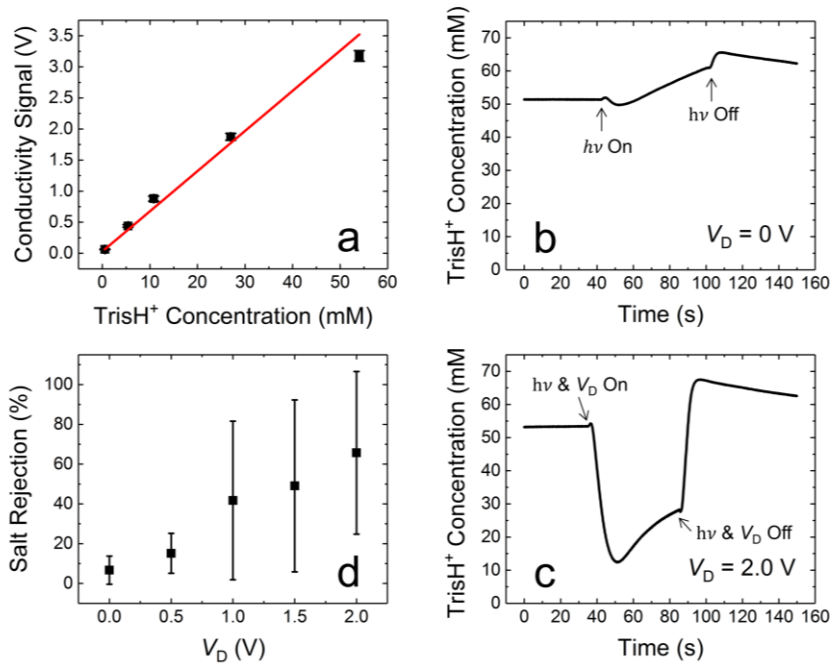

Figure 3.3: (a) A calibration curve relating solution conductivity to the concentration of $TrisH^+$ in the microelectrochemical device. For this experiment, 40 µL and 34 µL of Tris buffer were added to the inlet and outlet reservoirs so that the PDF flow rate was the same as the rest of the experiments in this figure. The horizontal axis is plotted in terms of the acidic form of Tris, because the basic form does not contribute to conductivity. The error bars represent the standard deviation from the mean for three measurements obtained using a single device. $R^2 = 0.98$. (b) Plot of the $TrisH^+$ concentration vs time for $V_D = 0$ V. (c) Plot of the $TrisH^+$ concentration vs time for $V_D = 2.0$ V. For (b) and (c), the measured solution conductivities were converted into equivalent $TrisH^+$ concentrations using the calibration curve in (a). Additionally, the light and V_D were turned on at 40 s and turned off at 1.0 min. (d) Plot of the percentage salt rejection (defined in the main text) vs V_D. The error bars represent the standard deviation from the mean for three measurements carried out using three independently fabricated devices. All conductivity data were measured using microbands *A* and *B* (Figure 3.2a) positioned ~180 µm downstream from the Pt cathode.

At t = 40 s, the photoanode was illuminated, and a few seconds later the downstream conductivity decreased. Earlier we showed that no electric field gradient forms when V_D = 0 V (Figure 3.2c), but a small current does pass (Figure 3.2d). Therefore, the slight decrease in the $TrisH^+$ concentration in Figure 3.3b must be due to a small amount of $TrisH^+$ being neutralized via eqs 2 and 3 and then transported to the conductivity electrodes by convection. Following this initial decrease in conductivity, there is a gradual increase in the apparent $TrisH^+$ concentration background. The observed increase is not real, however, but rather we believe it arises from an increase in conductivity due to heating of the solution by the Hg light. Specifically, the temperature increase results in a decrease in solution viscosity, a corresponding increase in ion mobility, and hence an increase in conductivity.[53] To confirm this hypothesis, we carried out an experiment identical to that represented in Figure 3.3b, but in the absence of faradaic reactions (i.e., at open circuit). The gradual change in apparent $TrisH^+$ concentration in this case (Figure 3.4) is nearly identical to that shown in Figure 3.3b. Finally, after 1.0 min of irradiation at V_D = 0 V, the light was turned off which stops $TrisH^+$ neutralization (eqs 2 and 3). Consequently, there is an immediate increase in the concentration of $TrisH^+$ followed by a slower decrease in the apparent concentration as the solution cools.

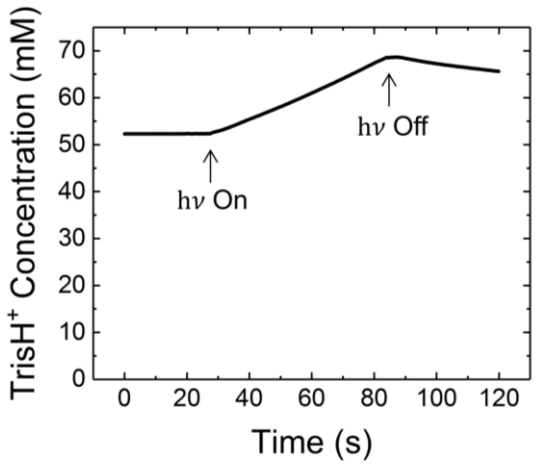

Figure 3.4: A control experiment showing how the apparent $TrisH^+$ concentration changes due to temperature. The concentration of Tris buffer in the microelectrochemical device was 100 mM (equivalent to 54.02 mM $TrisH^+$) at pH 8.0. The apparent concentration $TrisH^+$ as a function of time was determined by measuring the solution conductivity and then converting to concentration units using the calibration curve in Figure 3.3a of the main text. This measurement was carried out like those in Figure3.3b and 3c in the main text, except no V_D was applied (i.e., the Pt cathode was at open circuit). The light was turned on at t = 30 s and turned off at t = 90 s. As discussed in the main text, the apparent increase in $TrisH^+$ concentration is due to radiative heating of the solution by the lamp.

Figure 3.3c is analogous to Figure 3.3b, except now V_D = 2.0 V, which is sufficient to generate a significant IDZ. The characteristic gradual changes in the apparent concentration of $TrisH^+$ arising from heating are observed, but the most noticeable feature is the dramatic decrease in $TrisH^+$ concentration when both V_D and the light are switched on. We attribute this important observation to formation of an IDZ (as demonstrated in Figure 3.2c) and concomitant accumulation of ions upstream of the conductivity electrodes (Illustration 1.3b). After the light is turned off, the conductivity signal sharply increases, corresponding to collapse of the IDZ.

Figure 3.3d is a histogram showing the percentage of salt rejected (i.e., blocked) by the IDZ as a function of V_D. The rejection percentage was calculated from data like that shown in Figures 3.3b and 3.3c, and specifically from the differences between the initial and lowest concentrations of $TrisH^+$. This method was used, because it minimizes background changes arising from heating. Unsurprisingly, there is a monotonic increase in salt rejection as V_D increases. We conclude that a more depleted IDZ minimizes the amount of charge carriers reaching the conductivity electrodes.

One obvious problem that remains to be resolved is the poor device-to-device reproducibility of this experiment. As mentioned previously, the very large error bars in Figure 3.3d arise in part from differences in PDF, which in turn arise from slight differences in the dimensions of the inlet and outlet reservoirs. Variations in the photoelectrochemical properties of the TiO_2 thin films are likely contributors to device-to-device variations in the salt rejection percentage.

To confirm the salt rejection findings determined by conductivity measurements and represented in Figure 3.3d, we also used fluorescent ion tracers to visualize pICP ion filtration. Fluorescent tracers have previously been used to visualize ion enrichment[30,33,35] and ion separation[36,37] in fICP, so it is a well-established methodology.

In the present case, the tracers were negatively charged microspheres. The pICP experiment was carried out as discussed in the context of Figure 3.3, except 0.027 w/v percent of carboxyl-functionalized microspheres were added to the 100 mM Tris buffer. When the TiO_2 photoanode was illuminated with V_D = 0 V, the microspheres moved downstream due to PDF (Figure 3.5a). However, when V_D was increased to 2.0 V and with the light on, the microspheres accumulated in the vicinity of the Pt cathode (Figure 3.5b). Subsequently, when V_D was turned off, the accumulated microspheres were released downstream due to convection and collapse of the IDZ (Figure 3.5c). This behavior is identical to that inferred from the conductivity measurements (i.e., Figure 3.3c).

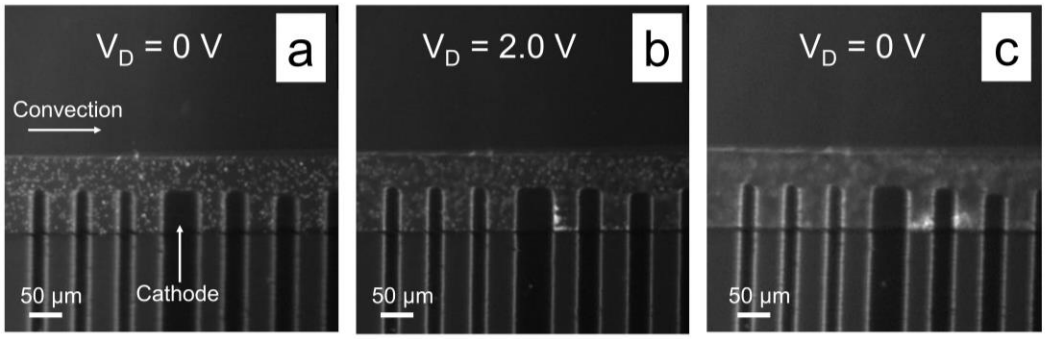

Figure 3.5: Fluorescence micrographs showing accumulation of microspheres near the Pt cathode. 40 µL and 34 µL of 100 mM Tris buffer (pH 8.0) with 0.027 w/v percent carboxyl-functionalized microspheres were added to inlet and outlet reservoirs to provide PDF. During the experiments, the Hg arc lamp continuously illuminated the TiO2 photoanode positioned at the bottom of inlet reservoir. All micrographs were taken chronologically while VD applied between the TiO2 photoanode and the Pt cathode changed from 0 V to 2.0 V and back to 0 V. The micrographs were taken (a) when VD was initially at 0 V, (b) 13 s after the VD was switched to 2.0 V, and (c) 1.0 s after the VD was changed back to 0 V. For the experiment, the 50 µm wide Pt cathode was placed in the middle of the microchannel to visually compare the flow with IDZ (lower-half channel) and the flow without IDZ (upper-half channel). Note that similar accumulation has been observed from the microelectrochemical device used for the other experiments (Figure 3.2a).

Chapter 4. Summary and Conclusions

In this study, we have shown that light energy can be used to manipulate the transport of ions, and we have provided a framework for understanding the mechanism. Specifically, a photoanode drives formation of an IDZ, and hence a local electric field gradient, at a Pt cathode. This IDZ accumulates charged species, as shown in Figure 3.5b, in essence removing them from the downstream solution.

Looking to the future, the findings reported here represent an important step toward developing an energy efficient, membraneless ion separation system specifically for sea water desalination. We have previously used fICP for this purpose,[40] thereby demonstrating the viability of the general methodology, but the use of photoelectrochemistry will minimize the required electrical energy. Our approach for accomplishing this goal is to generate the IDZ by photooxidizing Cl^-, which of course is abundant in sea water. The key to successful implementation will be to find a suitable anode/cathode pair that selectively oxidizes Cl^- in the presence of water oxidation. Leading candidates are the types of dimensionally stable anodes widely used in chlor-alkali industry,[54,55] coupled to an appropriate photocathode. The results of these experiments will be reported in due course.

References

(1) Li, M.; Anand, R. K. Recent Advancements in Ion Concentration Polarization. *Analyst* **2016**, *141*, 3496–3510.

(2) A. Zangle, T.; Mani, A.; G. Santiago, J. Theory and Experiments of Concentration Polarization and Ion Focusing at Microchannel and Nanochannel Interfaces. *Chemical Society Reviews* **2010**, *39*, 1014–1035.

(3) Kim, S. J.; Song, Y.-A.; Han, J. Nanofluidic Concentration Devices for Biomolecules Utilizing Ion Concentration Polarization: Theory, Fabrication, and Applications. *Chem. Soc. Rev.* **2010**, *39*, 912–922.

(4) Dai, J.; Ito, T.; Sun, L.; Crooks, R. M. Electrokinetic Trapping and Concentration Enrichment of DNA in a Microfluidic Channel. *J. Am. Chem. Soc.* **2003**, *125*, 13026–13027.

(5) Pu, Q.; Yun, J.; Temkin, H.; Liu, S. Ion-Enrichment and Ion-Depletion Effect of Nanochannel Structures. *Nano Lett.* **2004**, *4*, 1099–1103.

(6) Wang, Y.-C.; Stevens, A. L.; Han, J. Million-Fold Preconcentration of Proteins and Peptides by Nanofluidic Filter. *Anal. Chem.* **2005**, *77*, 4293–4299.

(7) Jin, X.; Joseph, S.; Gatimu, E. N.; Bohn, P. W.; Aluru, N. R. Induced Electrokinetic Transport in Micro−Nanofluidic Interconnect Devices. *Langmuir* **2007**, *23*, 13209–13222.

(8) Dhopeshwarkar, R.; Crooks, R. M.; Hlushkou, D.; Tallarek, U. Transient Effects on Microchannel Electrokinetic Filtering with an Ion-Permselective Membrane. *Anal. Chem.* **2008**, *80*, 1039–1048.

(9) Kwak, R.; Kim, S. J.; Han, J. Continuous-Flow Biomolecule and Cell Concentrator by Ion Concentration Polarization. *Anal. Chem.* **2011**, *83*, 7348–7355.

(10) Han, S. I.; Hwang, K. S.; Kwak, R.; Lee, J. H. Microfluidic Paper-Based Biomolecule Preconcentrator Based on Ion Concentration Polarization. *Lab Chip* **2016**, *16*, 2219–2227.

(11) Gong, M. M.; Nosrati, R.; San Gabriel, M. C.; Zini, A.; Sinton, D. Direct DNA Analysis with Paper-Based Ion Concentration Polarization. *J. Am. Chem. Soc.* **2015**, *137*, 13913–13919.

(12) Cheow, L. F.; Han, J. Continuous Signal Enhancement for Sensitive Aptamer Affinity Probe Electrophoresis Assay Using Electrokinetic Concentration. *Anal. Chem.* **2011**, *83*, 7086–7093.

(13) Yeh, S.-H.; Chou, K.-H.; Yang, R.-J. Sample Pre-Concentration with High Enrichment Factors at a Fixed Location in Paper-Based Microfluidic Devices. *Lab Chip* **2016**, *16*, 925–931.

(14) Kim, S. J.; Ko, S. H.; Kang, K. H.; Han, J. Direct Seawater Desalination by Ion Concentration Polarization. *Nat. Nanotech* **2013**, *8*, 609–609.

(15) D. MacDonald, B.; M. Gong, M.; Zhang, P.; Sinton, D. Out-of-Plane Ion Concentration Polarization for Scalable Water Desalination. *Lab Chip* **2014**, *14*, 681–685.

(16) Martinez, A. W.; Phillips, S. T.; Whitesides, G. M.; Carrilho, E. Diagnostics for the Developing World: Microfluidic Paper-Based Analytical Devices. *Anal. Chem.* **2010**, *82*, 3–10.
(17) Cunningham, J. C.; DeGregory, P. R.; Crooks, R. M. New Functionalities for Paper-Based Sensors Lead to Simplified User Operation, Lower Limits of Detection, and New Applications. *Annu. Rev. Anal. Chem* **2016**, *9*, 183–202.
(18) Cho, I.; Yong Sung, G.; Jae Kim, S. Overlimiting Current through Ion Concentration Polarization Layer: Hydrodynamic Convection Effects. *Nanoscale* **2014**, *6*, 4620–4626.
(19) Yossifon, G.; Chang, H.-C. Selection of Nonequilibrium Overlimiting Currents: Universal Depletion Layer Formation Dynamics and Vortex Instability. *Phys. Rev. Lett.* **2008**, *101*, 254501.
(20) Kwak, R.; Pham, V. S.; Lim, K. M.; Han, J. Shear Flow of an Electrically Charged Fluid by Ion Concentration Polarization: Scaling Laws for Electroconvective Vortices. *Phys. Rev. Lett.* **2013**, *110*, 114501.
(21) Rubinstein, S. M.; Manukyan, G.; Staicu, A.; Rubinstein, I.; Zaltzman, B.; Lammertink, R. G. H.; Mugele, F.; Wessling, M. Direct Observation of a Nonequilibrium Electro-Osmotic Instability. *Phys. Rev. Lett.* **2008**, *101*, 236101.
(22) Kim, S. J.; Wang, Y.-C.; Lee, J. H.; Jang, H.; Han, J. Concentration Polarization and Nonlinear Electrokinetic Flow near a Nanofluidic Channel. *Phys. Rev. Lett.* **2007**, *99*, 44501.
(23) Jännig, O.; Nguyen, N.-T. A Polymeric High-Throughput Pressure-Driven Micromixer Using a Nanoporous Membrane. *Microfluid Nanofluidics* **2011**, *10*, 513–519.
(24) Choi, E.; Kwon, K.; Lee, S. J.; Kim, D.; Park, J. Non-Equilibrium Electrokinetic Micromixer with 3D Nanochannel Networks. *Lab Chip* **2015**, *15*, 1794–1798.
(25) Sun, G.; Senapati, S.; Chang, H.-C. High-Flux Ionic Diodes, Ionic Transistors and Ionic Amplifiers Based on External Ion Concentration Polarization by an Ion Exchange Membrane: A New Scalable Ionic Circuit Platform. *Lab Chip* **2016**, *16*, 1171–1177.
(26) Fosdick, S. E.; Knust, K. N.; Scida, K.; Crooks, R. M. Bipolar Electrochemistry. *Angew. Chem. Int. Ed.* **2013**, *52*, 10438–10456.
(27) Loget, G.; Zigah, D.; Bouffier, L.; Sojic, N.; Kuhn, A. Bipolar Electrochemistry: From Materials Science to Motion and Beyond. *Acc. Chem. Res.* **2013**, *46*, 2513–2523.
(28) Anand, R. K.; Sheridan, E.; Knust, K. N.; Crooks, R. M. Bipolar Electrode Focusing: Faradaic Ion Concentration Polarization. *Anal. Chem.* **2011**, *83*, 2351–2358.
(29) Mavré, F.; Anand, R. K.; Laws, D. R.; Chow, K.-F.; Chang, B.-Y.; Crooks, J. A.; Crooks, R. M. Bipolar Electrodes: A Useful Tool for Concentration, Separation, and Detection of Analytes in Microelectrochemical Systems. *Anal. Chem.* **2010**, *82*, 8766–8774.

(30) Dhopeshwarkar, R.; Hlushkou, D.; Nguyen, M.; Tallarek, U.; Crooks, R. M. Electrokinetics in Microfluidic Channels Containing a Floating Electrode. *J. Am. Chem. Soc.* **2008**, *130*, 10480–10481.
(31) K. Anand, R.; Sheridan, E.; Hlushkou, D.; Tallarek, U.; M. Crooks, R. Bipolar Electrode Focusing: Tuning the Electric Field Gradient. *Lab Chip* **2011**, *11*, 518–527.
(32) Sheridan, E.; Hlushkou, D.; Anand, R. K.; Laws, D. R.; Tallarek, U.; Crooks, R. M. Label-Free Electrochemical Monitoring of Concentration Enrichment during Bipolar Electrode Focusing. *Anal. Chem.* **2011**, *83*, 6746–6753.
(33) Perdue, R. K.; Laws, D. R.; Hlushkou, D.; Tallarek, U.; Crooks, R. M. Bipolar Electrode Focusing: The Effect of Current and Electric Field on Concentration Enrichment. *Anal. Chem.* **2009**, *81*, 10149–10155.
(34) Anand, R. K.; Sheridan, E.; Knust, K. N.; Crooks, R. M. Bipolar Electrode Focusing: Faradaic Ion Concentration Polarization. *Anal. Chem.* **2011**, *83*, 2351–2358.
(35) Sheridan, E.; Hlushkou, D.; Knust, K. N.; Tallarek, U.; Crooks, R. M. Enrichment of Cations via Bipolar Electrode Focusing. *Anal. Chem.* **2012**, *84*, 7393–7399.
(36) N. Knust, K.; Sheridan, E.; K. Anand, R.; M. Crooks, R. Dual-Channel Bipolar Electrode Focusing: Simultaneous Separation and Enrichment of Both Anions and Cations. *Lab Chip* **2012**, *12*, 4107–4114.
(37) Laws, D. R.; Hlushkou, D.; Perdue, R. K.; Tallarek, U.; Crooks, R. M. Bipolar Electrode Focusing: Simultaneous Concentration Enrichment and Separation in a Microfluidic Channel Containing a Bipolar Electrode. *Anal. Chem.* **2009**, *81*, 8923–8929.
(38) Sheridan, E.; N. Knust, K.; M. Crooks, R. Bipolar Electrode Depletion: Membraneless Filtration of Charged Species Using an Electrogenerated Electric Field Gradient. *Analyst* **2011**, *136*, 4134–4137.
(39) Scida, K.; Sheridan, E.; M. Crooks, R. Electrochemically-Gated Delivery of Analyte Bands in Microfluidic Devices Using Bipolar Electrodes. *Lab Chip* **2013**, *13*, 2292–2299.
(40) Knust, K. N.; Hlushkou, D.; Anand, R. K.; Tallarek, U.; Crooks, R. M. Electrochemically Mediated Seawater Desalination. *Angew. Chem. Int. Ed.* **2013**, *52*, 8107–8110.
(41) Li, X.; Luo, L.; Crooks, R. M. Faradaic Ion Concentration Polarization on a Paper Fluidic Platform. *Anal. Chem.* **2017**, *89*, 4294–4300.
(42) Shackman, J. G.; Ross, D. Counter-Flow Gradient Electrofocusing. *Electrophoresis* **2007**, *28*, 556–571.
(43) Zhu, F.; Hayes, M. A. Exploring Gradients in Electrophoretic Separation and Preconcentration on Miniaturized Devices. *Separations* **2016**, *3*, 12.
(44) McDonald, J. C.; Duffy, D. C.; Anderson, J. R.; Chiu, D. T.; Wu, H.; Schueller, O. J. A.; Whitesides, G. M. Fabrication of Microfluidic Systems in Poly(dimethylsiloxane). *Electrophoresis* **2000**, *21*, 27–40.

(45) Zhou, B.; Jiang, X.; liu, Z.; Shen, R.; Rogachev, A. V. Preparation and Characterization of TiO2 Thin Film by Thermal Oxidation of Sputtered Ti Film. *Mater. Sci. Semicond. Process.* **2013**, *16*, 513–519.
(46) Shadpour, H.; Hupert, M. L.; Patterson, D.; Liu, C.; Galloway, M.; Stryjewski, W.; Goettert, J.; Soper, S. A. Multichannel Microchip Electrophoresis Device Fabricated in Polycarbonate with an Integrated Contact Conductivity Sensor Array. *Anal. Chem.* **2007**, *79*, 870–878.
(47) Tanyanyiwa, J.; Leuthardt, S.; Hauser, P. C. Conductimetric and Potentiometric Detection in Conventional and Microchip Capillary Electrophoresis. *Electrophoresis* **2002**, *23*, 3659–3666.
(48) Gratzel, M. Photoelectrochemical Cells. *Nature* **2001**, *414*, 338–344.
(49) Fujishima, A.; Rao, T. N.; Tryk, D. A. Titanium Dioxide Photocatalysis. *J. Photochem. Photobiol. C: Photochem. Rev.* **2000**, *1*, 1–21.
(50) Tafalla, D.; Salvador, P.; Benito, R. M. Kinetic Approach to the Photocurrent Transients in Water Photoelectrolysis at N - TiO2 Electrodes II . Analysis of the Photocurrent-Time Dependence. *J. Electrochem. Soc.* **1990**, *137*, 1810–1815.
(51) Hidalgo, D.; Bocchini, S.; Fontana, M.; Saracco, G.; Hernández, S. Green and Low-Cost Synthesis of PANI–TiO 2 Nanocomposite Mesoporous Films for Photoelectrochemical Water Splitting. *RSC Advances* **2015**, *5*, 49429–49438.
(52) Reier, T.; Oezaslan, M.; Strasser, P. Electrocatalytic Oxygen Evolution Reaction (OER) on Ru, Ir, and Pt Catalysts: A Comparative Study of Nanoparticles and Bulk Materials. *ACS Catalysis* **2012**, *2*, 1765–1772.
(53) Barron, J., J.; Ashton, C. *The Effect of Temperature on Conductivity Measurement*; 2005.
(54) Ferro, S.; De Battisti, A. Electrocatalysis and Chlorine Evolution Reaction at Ruthenium Dioxide Deposited on Conductive Diamond. *J. Phys. Chem. B* **2002**, *106*, 2249–2254.
(55) Rasmus K. B. Karlsson; Hansen, H. A.; Bligaard, T.; Cornell, A.; Pettersson, L. G. M. Ti Atoms in Ru0.3Ti0.7O2 Mixed Oxides Form Active and Selective Sites for Electrochemical Chlorine Evolution. *Electrochim. Acta* **2014**, *146*, 733–740.